The relation between measurement and visibility of anisotropy effects in tempered glass. A case study.

Autoren:

Steffen Dix[1], Christian Schuler[1], Stefan Kolling[2], Jens Schneider[3]
[1] Institute for Material and Building Research, University of Applied Science, Munich, Germany
[2] Institute of Mechanics and Materials, THM University of Applied Sciences, Giessen, Germany
[3] Institute of Structural Mechanics and Design, Technische Universität Darmstadt, Darmstadt, Germany

Keywords:

Glass stress, Thermal Tempering, Quality control, Photoelasticity, Anisotropy

Kontakt:

Steffen Dix
Institut für Material-und Bauforschung
Karlstraße 6
80333 München
sdix@hm.edu

Abstract

Optical anisotropy effects in tempered glass can affect the transparency of glass building envelopes in the form of iridescence. Birefringence is created in the standard tempering process and results from even the smallest principal stress differences across the thickness of the glass. Currently, no standard or guideline exists for evaluating optical anisotropy effects in tempered glass. In recent years, photoelastic methods have been developed for full-field, non-destructive measurement of optical retardation caused by anisotropy effects. This study focuses on whether and how the retardation measurements correlate with the visual anisotropy effects under natural daylight in reality. Therefore, quantitative retardation measurements were first performed on various glass panes, followed by qualitative studies to correlate the visibility of the anisotropy effects in an outdoor test facility. The investigation shows that the quantitative measurement of optical retardation and the presented evaluation methods allow the objective evaluation of anisotropy effects.

1 Introduction

Anisotropy effects are visual color appearances (iridescence) that mainly occur in tempered glass and can be perceived as gray to colored patterns under polarized light incidence and certain viewing angles in the facade. They result from non-uniformly induced residual stresses in the tempering process [1–3].
In recent years, measurement systems have been developed to quantify anisotropy effects by measuring optical retardation [1, 4–6]. This study aimed to derive a correlation between the subjective visual anisotropy effects and the values and patterns determined in the retardation images. In addition, it was examined whether the evaluation methods of the quantitative measurements can determine the anisotropy quality of the glass panes in reality.
For this purpose, photoelastic, full-field measurements were first performed on a selection of tempered glass panes. The same samples were then installed in an outdoor test facility and observed and subjectively evaluated under specific lighting scenarios.

2 Basics and state of research

2.1. Optical anisotropy effects

Transparent materials, such as glass or plastics alter their optical properties under mechanical stress. They become directionally dependent (anisotropic) and are thus birefringent. The optical phenomenon of birefringence can be explained with the aid of photoelasticity. When a polarized light beam hits a birefringent medium, it splits in the plane into two vectors according to the two principal stress directions σ1 and σ2. After passing the birefringent medium, the two components receive an optical retardation δ due to the stress state, which is directly related to the interference colors of the anisotropy effects, see Fig. 1. Detailed theoretical principles can be found in [7, 8].
Tempered glass, which is subjected to a residual stress state by heat treatment, may contain more or less visible anisotropy effects depending on the homogeneity of the tempering process. In addition to the uniformity of the induced residual stress, i.e., the difference between the two principal stresses σ1 and σ2, the material constant C and the thickness t are decisive factors in the occurrence of retardation. According to [7], this relation can be described mathematically by the stress differences integrated over the glass thickness:

$$\delta = C \int_{z=0}^{z=t} (\sigma_1(z) - \sigma_2(z)) dz \quad (1)$$

This means: The thicker the glass assembly of a glazing, the more likely retardation accumulates over the thickness, leading to more colorful interference colors that can appear as anisotropy effects under partially polarized daylight, see Fig. 1. Further factors that increase the probability of visible anisotropy effects can be found in the current guideline [2].

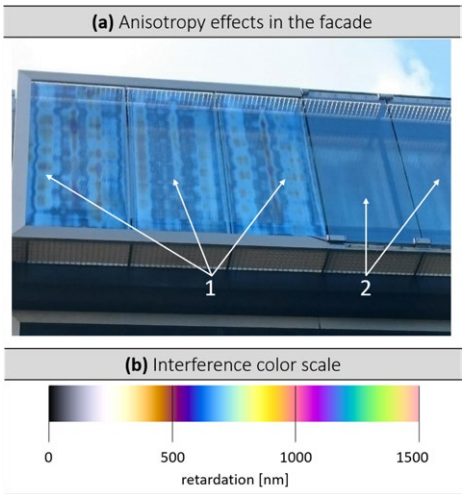

Figure 1: (a) Facade with tempered glass panes, strong (arrows 1) and weak (arrows 2) optical anisotropy effects, image taken without a polarizing filter in Luxembourg (©Ruth Kasper from [7]. (b) Interference color scale according to Michel-Lévy analytically calculated in [1].

2.2. Photoelastic measurement methods

Photoelasticity includes various techniques by which stresses in transparent materials can be made qualitatively visible and quantitatively measurable. Classical photoelastic methods, as explained in [9] and [10], have been extended and applied on large-scale tempered glass panes in the last six years [1, 4–6]. In this paper, the so-called phase-shifting technique is used.
The phase-shifting technique has the advantage that it can be used directly without generating a calibration table to detect both retardation and the orientation of the stress (azimuth) in transparent media. The photoelastic setup is also known as a

polarimeter, using the compensation principle according to Sénarmont or Tardy [11]. With the advancement from polarimeter with rotating optical elements [3, 12] to devices whose analyzers can analyze multiple planes of polarization (0°, 45°, 90°, and 135°) simultaneously [5, 13]. Thereby generating real-time retardation images, the technique is also applied to measure anisotropy effects in tempered glass.

In principle, the following applies to this measurement technique: With the knowledge of the alignment of the optical elements (polarizer, quarter-wave plates, and analyzer), the retardation δ and the azimuth angle φ can be calculated from the intensity of the light using the Mueller matrix, see [5, 14]. For the experimental investigations in section 3, the measuring system Strainscanner from the company ilis GmbH in Erlangen was used, see Fig. 2. In our case, it has a measurement range from 0 to 120 nm with a resolution of 2 mm per pixel.

2.3. Evaluation methods

In [15], the current digital evaluation methods are presented in detail. However, before the retardation images are evaluated according to these, evaluation zones are defined, excluding areas with unavoidable high differences in retardation. For the tests carried out in this paper, zone E+M was chosen. This zone consists of the pane area minus 50 mm from the edges.

The 95% quantile value $x0_{,95}$ is determined from the empirical distribution function and states that 95% of the existing retardation values are smaller than the determined value. A lower value stands for a better optical quality of the glass pane.

The isotropy value Iso_{75} represents the percentage of the glass area below a threshold value T (here 75 nm). For this purpose, the retardation image is divided into areas with values greater than (1) and less or equal to T (0) and converted into a binary image. With consideration of the orientation ($Iso_{75,A}$), areas are additionally excluded (0), which have azimuth angles of ± 45 °, since these become less visible with horizontal or vertical facade installation [3]. The higher the isotropy value the better the anisotropy quality of the glass pane.

The texture features Contrast (C) and Cluster Prominence (CP) based on texture analysis can capture the spatial distribution of the retardation in addition to $x_{0,95}$ und Iso_{75}. C is an indicator of homogeneity, and CP detects coherent areas. The lower the values, the more homogeneous and better the anisotropy quality. The final setting parameters from [15] were used to calculate the results.

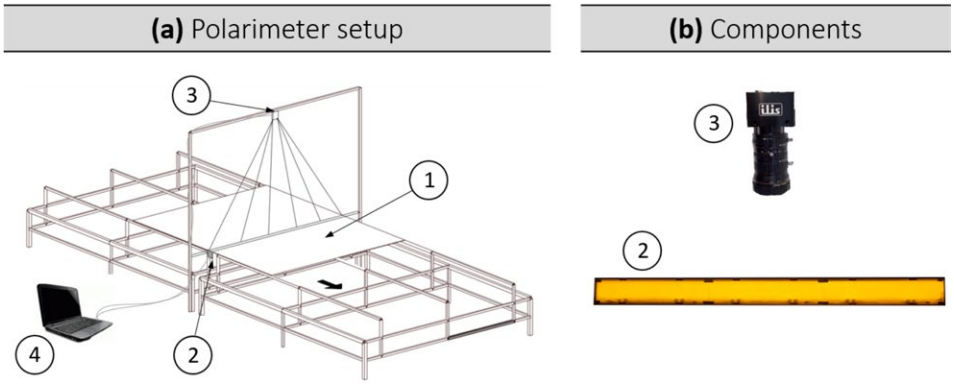

Figure 2: (a) Polarimeter setup and components (b): 1. Glass sample; 2. Monochromatic light source with circular polarizer; 3. Polarization camera as analyzer.4. Computer for controlling the camera and light source, as well as for image processing and evaluation. 2 and 3 are components of the strainscanner from ilis GmbH Erlangen.

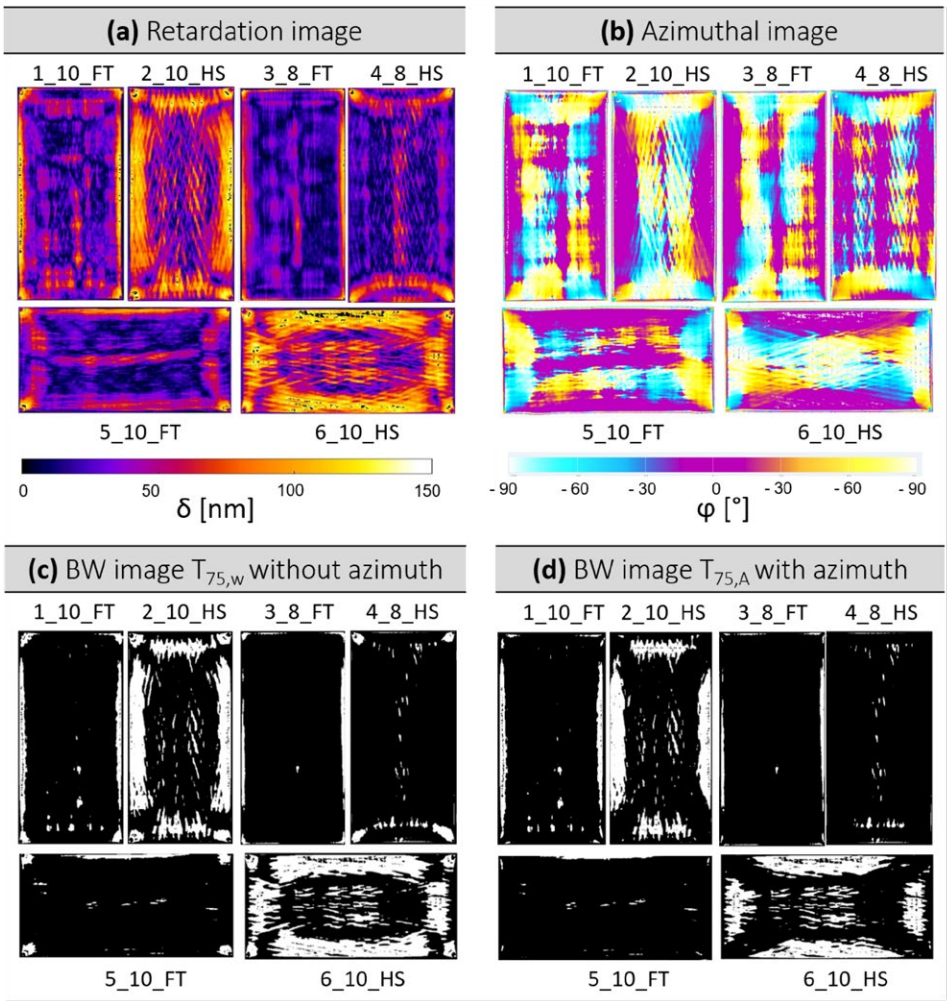

Figure 3: False-Color Plot of retardation image (a), azimuthal image. (b). BW Images without (c) and with consideration of azimuthal angle (d).

3 Quantitative measurements

In the present study, full-field, photoelastic measurements of tempered glass panes were performed using the Strainscanner in the laboratory. Based on the generated data, retardation and azimuthal angle, optical anisotropy effects caused by residual stress differences were objectively evaluated using the presented evaluation methods. For this purpose, six tempered glass panes with different thicknesses (8 mm and 10 mm) and tempering levels (Fully tempered (FT) and heat-strengthened (HS)) were chosen. The monolithic panes with a width of 750 mm and a length of 1500 mm were individually scanned in the laboratory under constant conditions. The measurement results are collected and shown in Fig. 3 (a) and (b) as false-color plots with respective scales. The arrangement of the samples is simultaneous to the installation situation in section 4. Fig. 3 (a) shows the

distribution of the optical retardation in the unit nm over the glass surface of the test samples. With the help of the colored scale, the reader can subjectively compare the specimen before evaluation based on the distribution and amount of retardation. For example, samples 2_10_HS and 6_10_HS contain obviously the highest retardations.
Fig. 3 (b) shows the spatial distribution of the azimuthal angle over the glass pane. The azimuthal angle is not displayed by default and therefore, the interpretation is unknown to the non-expert reader. However, it is recognizable that the samples show coherent areas with the same orientations. It is noticeable that high retardations (orange and yellow) often correlate with orientations around 0° and ± 90° (white and magenta). Azimuthal angles around ± 45° (aquamarine and yellow) mainly occur in the corner of the panes. Fig. 3 (c) and (d) show the application of the isotropy value at a threshold of 75 nm without (c) and with (d) consideration of the azimuthal angle. Comparing the two binary images (BW), they obviously differ primarily in the corner.
Table 1 compares the results of the evaluation methods presented in section 2.3. Based on these, the glass panes were rated from one to six. The samples with the worst rating are 2_10_HS and 6_10_HS, this is also displayed by the BW image in Fig. 3, regardless of with or without orientation.

4 Qualitative observations at the outdoor test facility

The outdoor test facility consists of a facade mounted on a pillar jib crane which can be rotated through 360°, see Fig. 4. The facade is made of a steel frame with movable mullions and transoms, allowing flexible arrangement of the glass panes. For this purpose, mounting rails from HALFEN GmbH and set-on-top profiles with a pressure plate system from RAICO GmbH were used.
The stationary test facility was launched on July 20th 2020, in Kissing, Germany. Since then, observations under different environmental conditions have been performed by the authors. In this paper, an exemplary day, September 09th 2020, was selected on which a very high degree of polarization (DoP) p of the sky was present. The DoP represents the proportion of polarized light in natural daylight. To increase the visibility of the anisotropy effects, a black light-absorbing background was added inside the facade.
In order to support the qualitative observations, simultaneous measurements of the Stokes Parameter [16], the DoP, and the polarizing angle θ were conducted with a self-constructed polarimeter, according to [17]. The generated quantitative measured values were calculated according to [16]:

Sample	Results evaluation methods					Rated
	$x_{0,95}$	Iso_{75}	$Iso_{75,A}$	C	CP	
	[nm]	[%]	[%]	[-]	[-]	[1-6]
1_10_FT	72	96	97	0,79	4,25	4
2_10_HS	111	71	78	1,55	10,71	5
3_8_FT	49	100	100	0,35	0,64	1
4_8_HS	71	97	98	0,71	2,55	3
5_10_FT	67	98	99	0,71	2,36	2
6_10_HS	123	58	71	1,94	13,30	6

Table 1: Results of different evaluation met hods for zone E+M. Rating of anisotropy quality based on the evaluation criteria.

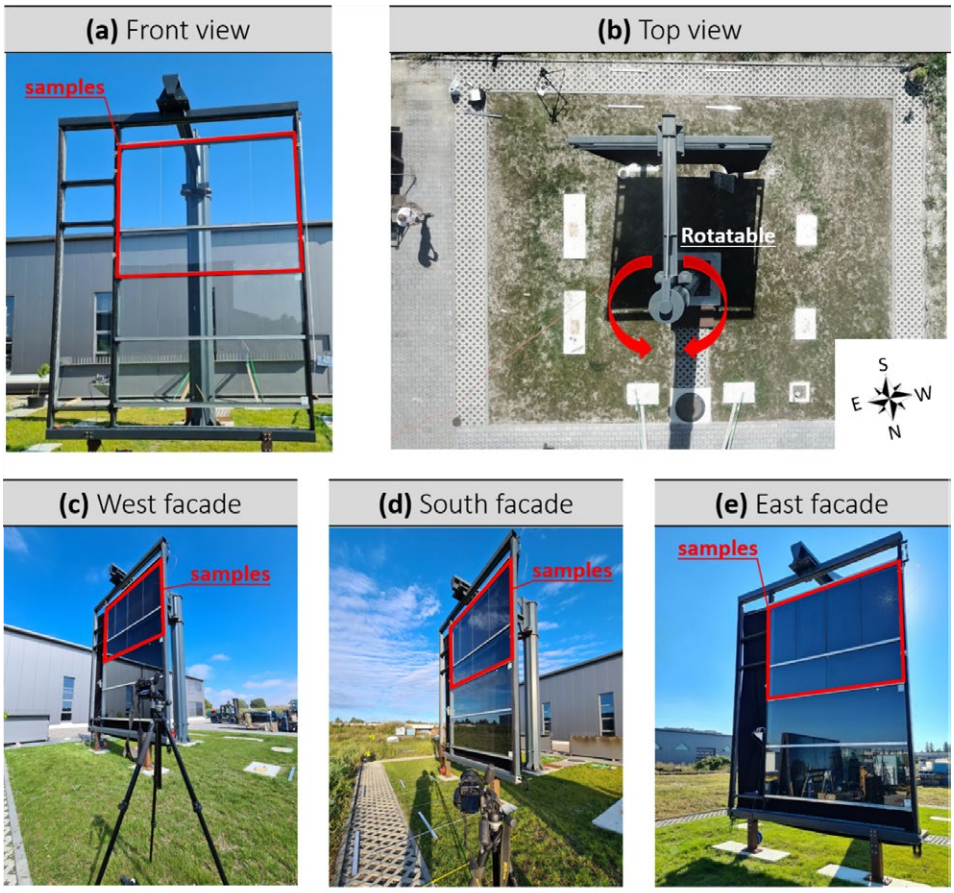

Figure 4: Outdoor test facility in Kissing, Germany under different viewing conditions (a, b) and facade orientation (c, d, e).

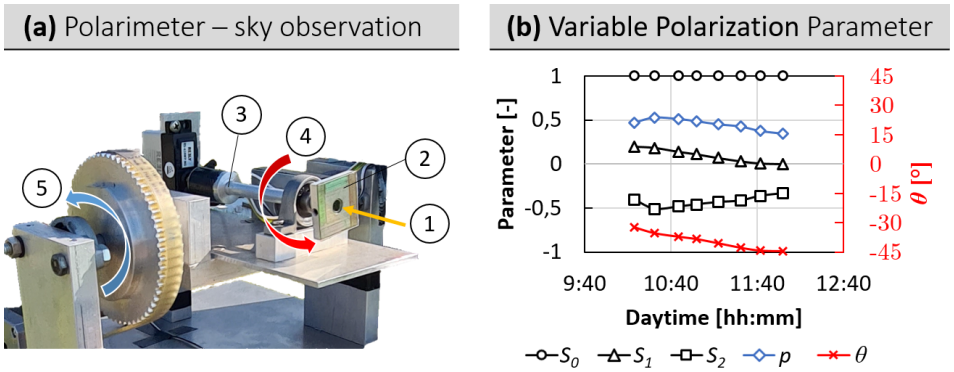

Figure 5: (a) Polarimeter to determine polarization parameter of skylight with: 1) Lightray; 2) Polarizer 3) Light sensor; 4) Rotation Polarizer – 180° 5) Angular solar distance – 90° rotation. (b) Polarization distribution of incoming skylight during observation in Brewster angle.

$$S_0 = I_x + I_y \quad (2)$$

$$S_1 = I_x - I_y \quad (3)$$

$$S_2 = I_{+45°} + I_{-45°} \quad (4)$$

$$\theta = \frac{1}{2}\tan^{-1}\frac{S_2}{S_1} \quad (5)$$

$$p = \frac{\sqrt{S_1^2+S_2^2}}{S_0} \quad (6)$$

Fig. 5 (a) displays the polarimeter, which was mounted perpendicular to the observation angle on the facade. The parameters of the incoming skylight polarization are calculated from measured intensity values I from different polarizer arrangements (**Ix, Iy, I45, I-45**). Fig. 5 (b) displays the skylight polarization data from measurements in the west facade orientation under Brewster Angle on September 09th, 2020. Fig. 6 shows the reflection image of the west facade taken under an angle close to the Brewster angle when the facade was oriented perpendicular to the sun. Under this worst-case scenario [18], maximum anisotropy effects were perceived by the author From Fig. 5 (b), it is noticeable that p decreases slightly towards noon, while θ clearly approaches the value 45°. It indicates that not only the degree of polarization p but especially the direction of the linear polarization θ play a decisive role in the evaluation of the perceptibility of anisotropy effects. The anisotropy quality now becomes apparent, grading from samples 3 and 5 with almost no effects, through samples 1 and 4 with slight effects, to samples 2 and 6 with clearly visible anisotropy effects. These appear as black-gray patterns in the reflection of the sky.

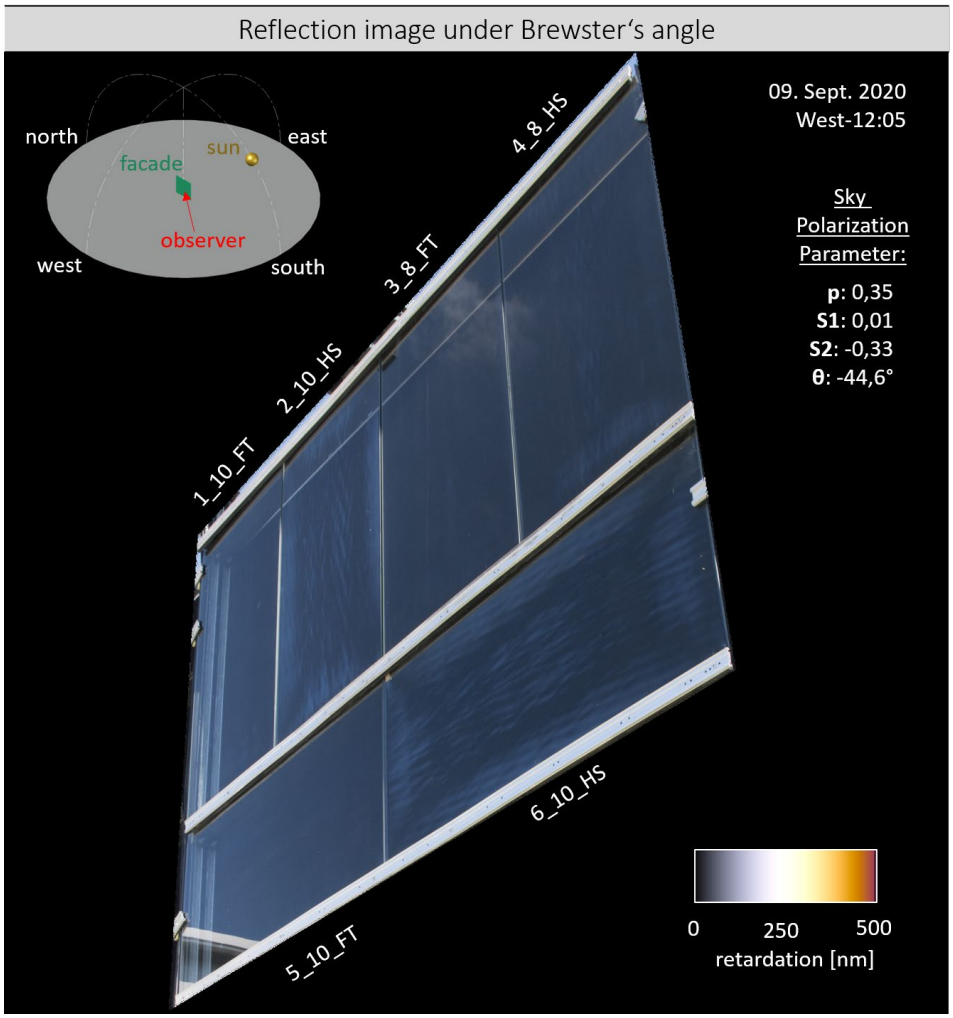

Figure 6: Reflection image of installed specimens in the outdoor test stand, position west facade. Recorded on September 09th 2020, at 12:05, without a polarizing filter at a DoP of 35% and polarization angle θ of -45°.

5 Comparison

Here, the results of the measurements from Section 3 are compared to the images taken at the outdoor test facility in Section 4. Before the actual comparison starts, the authors indicate the influence of the polarization data. Depending on the level of **p** and the orientation **θ**, the anisotropy patterns become less (Fig. 7 a) or more visible (Fig. 7 b).
Comparing the reflection image (b) with the retardation image (c) and the BW image (d), it becomes clear that they nearly entirely match. High retardations in (c) are also detectable in (b), and the pattern in (b) correlates with the pattern of the BW image at a threshold of 75 nm (d). This result can also be applied to the other samples. For this purpose, Fig. 3 (a and c) must be compared with Fig. 6. The rating from Table 1 also corresponds to the visibility in the actual installation situation under the worst conditions. It could therefore be shown that the visible anisotropy effects can be accurately reproduced with the quantitative measurements.

6 Summary and outlook

In the presented paper, optical anisotropy effects in tempered architectural glass were quantified by full-field photoelastic measurements, evaluated by different methods of image processing and observed under natural daylight in an outside test facility.
The investigations showed that the retardation images acquired in the laboratory correlate with the anisotropy effects occurring under real installation conditions. Observing the visual effects under natural light, the simultaneous measurement of the degree of polarization and the orientation of linear polarization θ was useful. The quantitative retardation measurement combined with the evaluation methods was recommended to assess the anisotropy quality of monolithic glass.
Future investigations will involve measurements on a large variety of tempered glass panes to provide a basis for the definition of limit values in the German guideline DIN SPEC 18198, which is currently being drafted. In addition, investigations on the outdoor test facility are planned to gather further knowledge on the visibility of anisotropy effects in monolithic and laminated glass.

7 References

[1] M. Illguth, C. Schuler und Ö. Bucak, „The effect of optical anisotropies on building glass façades and its measurement methods", Frontiers of Architectural Research, Jg. 4, Nr. 2, S. 119–126, 2015, doi: 10.1016/j.foar.2015.01.004.
[2] H. Dehner und A. Schweitzer, „Thermisch vorgespannte Gläser für den Architekturbereich ohne optisch wahrnehmbare Anisotropien" in Glasbau 2015, B. Weller und S. Tasche, Hg., Berlin: Ernst & Sohn, 2015.
[3] FKG, „Technical Note FKG 01/2019 -The visual quality of glass in building – anisotropies in heat treated flat glass", 2019.
[4] R. Decourcelle, G. Kaminski und Serruys F., „Controlling Anisotropy" in Glass Performing Days, Tampere, 2017, S. 157–160.
[5] H. Katte und G. Saur, „Inline measurement of residual stresses in large format objects.", Glass Worldwide, Nr. 77, 84,86, 2018.
[6] K. Vogel, „Optimized Furnace Settings with New Anisotropy and Haze Measurement Methods." in Glass Performing Days, 2019. [Online]. Verfügbar unter: https://www.glassonweb.com/article/

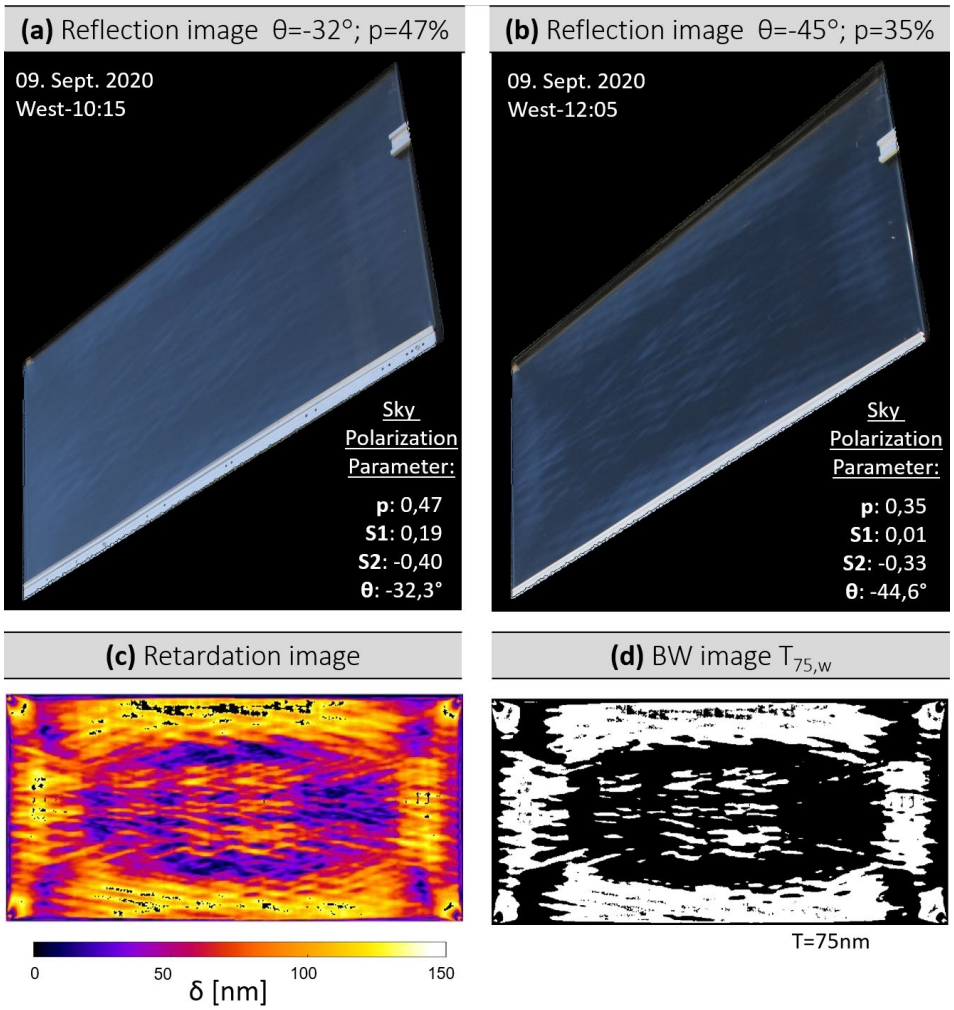

Figure 7: (a) and (b) reflection image of sample 6_10_HS in outdoor test facility, position west facade at 10:15 o´clock with θ=-32° and p = 47 % (a) , as well as at 12:05 o´clock with θ=-45° and p = 35 % (b). For comparison, retardation image (c) and BW image (d) of sample 6_10_HS.

optimized-furnace-settings-with-new-anisotropy-and-haze-measurement-methods
[7] H. Aben und C. Guillemet, Photoelasticity of glass. Berlin: Springer, 1993.
[8] B. Schaaf, P. Di Biase, M. Feldmann, C. Schuler und S. Dix, „Full-surface and Non-destructive Quality Control and Evaluation by Using Photoelastic Methods" in Glass Performing Days, Tampere, 2017, S. 130–134.
[9] R. Vivek und K. Ramesh, „A novel method for the evaluation of stress-optic coefficient of commercial float glass", Measurement, Jg. 87, S. 13–20, 2016, doi: 10.1016/j.measurement.2016.03.014.
[10] A. Ajovalasit, G. Petrucci und M. Scafidi, „Review of RGB photoelasticity", Optics and Lasers in Engineering, Jg. 68, S. 58–73, 2015, doi: 10.1016/j.optlaseng.2014.12.008.
[11] K. Ramesh, Digital photoelasticity: Advanced techniques and applications. Berlin: Springer, 2000.
[12] J. R. Lesniak und M. J. Zickel, „Applications of automated grey-field polariscope." in Proceedings of the SEM spring conference on experimental and applied mechanics, 1998, S. 298–301.
[13] M. Honlet, J. R. Lesniak, B. R. Boyce und G. C. Calvert, „Real-time photoelastic stress analysis – a new dynamic photoelastic method for non-destructive testing", insight, Jg. 46, Nr. 4, S. 193–195, 2004, doi: 10.1784/insi.46.4.193.55650.
[14] T. Onuma und Y. Otani, „A development of two-dimensional birefringence distribution measurement system with a sampling rate of 1.3MHz", Optics Communications, Jg. 315, S. 69–73, 2014, doi: 10.1016/j.optcom.2013.10.086.
[15] S. Dix, P. Müller, C. Schuler, S. Kolling und J. Schneider, „Digital image processing methods for the evaluation of optical anisotropy effects in tempered architectural glass using photoelastic measurements", Glass Struct Eng, Jg. 11, Nr. 6, S. 10, 2021.
[16] H. Fujiwara, Spectroscopic ellipsometry: Principles and applications. Chichester: Wiley, 2009.
[17] C. P. Abayaratne und V. Bandara, „A low-cost polarimeter for an undergraduate laboratory to study the polarization pattern of skylight", American Journal of Physics, Jg. 85, Nr. 3, S. 232–238, 2017, doi: 10.1119/1.4971159.
[18] S. Dix, K. Thiele, L. Efferz, C. Schuler, J. Schneider und S. Kolling, „Test facilities and concept for the evaluation of optical anisotropy effects in tempered glass" in Structures and Architecture A Viable Urban Perspective?, P. J. Cruz und M. F. Hvejsel, Hg., London: CRC Press, 2022, S. 1096–1104, doi: 10.1201/9781003023555-131.